# In-droplet electromechanical cell lysis and enhanced enzymatic assay driven by ion concentration polarization

Sungu Kim[a,d,‡], Aparna Krishnamurthy[b,‡], Pooja Kasiviswanathan[c], Baskar Ganapathysubramanian[a], and Robbyn K. Anand*[b]

[a]Department of Mechanical Engineering, Iowa State University, Ames, IA 50011.
[b]Department of Chemistry, Iowa State University, Ames, IA 50011.
[c]Microbiology Undergraduate Program, Iowa State University, Ames, IA, 50011.
[d]Department of Mechanical Engineering, Stanford University, Stanford, CA 94305 (current affiliation).
[‡]Equal contribution

**ABSTRACT:** Droplets enable the encapsulation of cells for their analysis in isolated domains. The study of molecular signatures (including genes, proteins, and metabolites) from few or single cells is critical for identifying key subpopulations. However, dealing with biological analytes at low concentrations requires long incubation times or amplification to achieve the requisite signal strength. Further, cell lysis requires additional chemical lysing agents or heat, which can interfere with assays. Here, we leverage ion concentration polarization (ICP) in droplets to rapidly lyse breast cancer cells within 2 s under a DC voltage bias of 30 V. Numerical simulations attribute cell lysis to ICP-based electric field and shear stress. We further achieve up to 19-fold concentration enrichment of an enzymatic assay product resulting from cell lysis, and a 3.8-fold increase in the reaction rate during enrichment. Our technique for sensitive in-droplet cell analysis provides scope for rapid, high-throughput detection of low-abundance intracellular analytes.

Droplet-based microfluidics has profoundly impacted applications ranging from single-cell analysis and biochemical assays to droplet-templated synthesis.[1] Several advancements in droplet generation and manipulation techniques have expanded the versatility of droplet microfluidic platforms to meet the demands of these applications.[2,3] Microfluidic droplets are phase-separated and can be tuned to handle minute sample volumes (fL to nL). Further, the ability to encapsulate bioparticles such as cells makes droplets ideal scaffolds for their analysis.

Techniques for the analysis of few or single cells are fundamental to cancer studies. Intratumor heterogeneity which is the cell-to-cell phenotypic or genotypic variability within tumor tissue, significantly contributes to cancer dynamics, drug resistance, and incomplete or redundant treatment efforts. Therefore, analyzing molecular signatures from individual cells is vital to evaluate the dynamic tumor microenvironment.[4–6] Several researchers have leveraged droplet microfluidic platforms to study biochemical reactions at the single-cell level. Yu et al. monitored matrix metalloproteinase (MMP) activity in monodisperse microdroplets encapsulating individual tumor cells.[7] Dhar et al. studied protease secretion from circulating tumor cells after their size-based purification and encapsulation within microdroplets.[8] However, often, the biochemical reactions in such applications either require additional chemical agents for enzyme up-regulation or require long incubation times for the enzyme to exhibit a detectable signal at its original abundance. These limitations necessitate the development of more sensitive in-droplet detection techniques that integrate analyte enrichment steps either before or during analysis.

Ion concentration polarization (ICP) has emerged as a powerful tool with analyte enrichment factors (EF) reaching up to a billion-fold in single-phase microfluidic platforms depending on the volume of sample swept.[9] ICP is the simultaneous enrichment and depletion of ions at the opposing ends of a nanochannel or ion-permselective membrane connecting two microscale compartments when subjected to a voltage bias. ICP has been employed by researchers to interface bioanalyte enrichment with droplet microfluidic workflows. For example, Chen et al. leveraged ICP to preconcentrate the protease MMP9 in a single phase before encapsulating the enriched analyte plug as highly concentrated microdroplets.[10] Their method significantly reduced the assay time and exhibited improved limits of detection. However, enriching the analyte prior to droplet encapsulation convolves the analyte signals. For example, if enzymes secreted from a cell cluster are enriched as a plug, the enzyme levels associated with individual cells remain unknown. Dittrich and coworkers demonstrated the electrophoretic in-droplet enrichment of small organic molecules and nucleic acids, and their subsequent separation into daughter droplets containing depleted and enriched analyte concentrations.[11] Their method integrates analyte enrichment with downstream droplet splitting to retrieve enriched and depleted daughter droplets. The reported technique involves linear electrophoretic separation of bioanalytes, and the mechanism is significantly distinct from that of ICP. Our group recently reported ICP-mediated in-droplet local concentration enrichment of small organic molecules ($BODIPY^{2-}$, Texas Red), mobility-based separation, and ion exchange in stationery droplets.[12] In-droplet ICP is a novel technique exhibiting salient features such as droplet-confined electric field gradient, electroconvective vortex formation, and enrichment of analytes into discrete pockets. These features can be harnessed to facilitate applications not only pertaining to bioanalysis but also

to the fields of separation science and droplet-templated synthesis.

Here, we report the in-droplet ICP-driven electromechanical lysis of breast cancer cells and enhancement in the sensitivity of a subsequent enzymatic assay. Specifically, ICP drives local increases in electric field strength and shear stress that mediate in-situ cell lysis, which in turn releases intracellular beta-galactosidase, used here as a model enzyme. The released enzyme reacts with its substrate, a fluorogenic reporter, present in the encompassing droplet medium to yield a fluorescent product. Enzyme activity is correlated to the rate of product formation, which is monitored by fluorescence imaging as the rate of change in the total fluorescence intensity in the droplet. In-droplet ICP was subsequently leveraged again during the enzymatic assay to provide two distinct advantages. First, the reaction rate during ICP is increased about 3.8 times by locally concentrating the enzyme and reagents to enable early detection. Second, local enrichment of the product amplifies the fluorescence signal, thereby improving the limit of detection (LOD) in terms of concentration by more than an order of magnitude. Under the conditions used here, up to a 19-fold increase in the maximum intensity (19-fold enrichment) compared to that without ICP is achieved. Unlike previously reported methods, in our method, ICP is implemented in pre-formed droplets, thereby preserving single- or few-cell isolation. Moreover, this method provides in-droplet on-demand cell lysis and lysate recovery without involving additional heat or chemical lysing agents that increase the complexity of droplet workflows and can interfere with reactions.

## MATERIALS AND METHODS

**Chemicals.** Texas Red dye-linked albumin was obtained from Molecular Probes (Eugene, OR). Nafion perfluorinated resin (20 wt% solution in lower aliphatic alcohols) was purchased from Sigma-Aldrich, (St. Louis, MO) and diluted with 200 proof ethanol (Fisher Scientific) in 1:3 ratio. Tris·HCl stock solution (1.0 M) obtained from Sigma-Aldrich, Inc. (St. Louis, MO, USA), was used to prepare Tris·HCl buffer at pH 8.1, concentration of 200.0 mM and conductivity of 9.8 mS/cm. The 200.0 mM Tris·HCl was used to fill the anodic and cathodic auxiliary channels of the device for all the experiments. All solutions were made in double deionized water (18.2 MΩ cm, Sartorius Arium Pro, Göttingen, Germany). Droplet (dispersed phase) compositions were distinct across different experiments and have been delineated under respective subsections. For the continuous phase, heavy mineral oil with 0.1 w/w% of Triton-X100 (Fisher bioreagents) and 3 w/w% of ABIL EM 90 (Evonik Industries, Essen, Germany) were used. Poly(dimethylsiloxane) (Sylgard 184 elastomer kit, Dow Corning Corp., Midland, MI) was used for device fabrication. Platinum electrodes (99.95%) were purchased from Strem Chemicals (Newburyport, MA). For enzymatic assays, Mg++ buffer comprising 0.001 mM $MgCl_2.6H_2O$ (Fisher) in 0.067 M beta-mercaptoethanol (MP Biomedicals, LLC, Solon, OH) was prepared.

**Device fabrication.** The device was fabricated following a similar fabrication protocol as our previous work.[12] Briefly, standard soft lithography techniques were used to fabricate poly(dimethylsiloxane) (PDMS) devices. Microscope glass slides were cleaned in a base bath containing 1:1:1 solution of hydrogen peroxide, ammonium hydroxide and double deionized (DDI) water at 90 °C for 1 h. Then, the slides were rinsed with 200 proof ethanol and dried with nitrogen gas. The PDMS chips with the design for Nafion membranes were reversibly bonded over the clean glass slides. Nafion solution (1:3 in ethanol) was then flow-patterned on the glass slide via capillary action along the PDMS microchannels. The slides were then subjected to soft baking at 65 °C for 30 min followed by curing at 95 °C for 10 min. The reversibly bonded chips were peeled off to reveal the Nafion membranes. A razor blade was used to cut off excess Nafion and ethanol was used to wipe away any residues. Next, the PDMS chips with microchannel designs were treated to air plasma (PDC-001, Harrick Plasma, Ithaca, NY) and irreversibly bonded over the Nafion-patterned slides. The assembled device was baked at 65 °C for more than 24 h to strengthen the bonding.

Details of the device dimensions and schematic representation of the device fabrication process are provided in Supporting Information, Note 1 and Figure S1, respectively. For all experiments, the droplet volume was maintained to be under, or ~1 nL. SEM images of the patterned membranes are included in the Supporting Information, Figure S2.

**Cell preparation.** MDA-MB-231 cells were obtained from ATCC (American Type Culture Collection, Manassas, VA; MDA-MB-231 ATCC HTB-26). Cells were cultured at 37 °C and 5% $CO_2$ in DMEM/F-12 (Dulbecco's Modified Eagle Medium/Nutrient Mixture F-12) cell culture medium obtained from Sigma-Aldrich, Inc. (St. Louis, MO, USA). The culture was supplemented with 10% fetal bovine serum obtained from ATCC. Cell cultures were passaged every 3-4 days to maintain cell confluence at less than 80%. Trypsin-EDTA (1X, 0.25%) was used to detach the adherent MDA-MB-231 cells from the floor of the culture flask. The contents from the flask were pelleted by centrifugation (1100 rpm, 5 min) and resuspended in a buffer solution. The buffer used to suspend cells was distinct between experiments and was either Dulbecco's Phosphate-Buffered Saline (1X DPBS, Corning®) with a pH 7.39 and conductivity 16.19 mS/cm, or a low conductivity buffer having pH 7.06 and conductivity 1210 $\mu$S/cm (comprising 10.0 mM sodium phosphate buffer, 8.0% sucrose, 0.1% BSA, and 0.3% dextrose). For the investigation of cell lysis, cells were stained using Calcein AM cell permeant dye obtained from Invitrogen™, ThermoFisher Scientific. The dye was solubilized in DMSO and added to the cell solution at a final concentration of 10.0 $\mu$g/mL. The cell-staining was carried out at an incubation temperature of 37 °C for 30 min. A cell countess (ThermoFisher Scientific) was used to measure the percentage of live cells in the solution. Cell encapsulation in droplets follows Poisson distribution and the cell concentration can be modulated (via dilution) to achieve single to multi-cell encapsulation (Supporting Information, Figure S3).

**Fluorescence Imaging.** All fluorescence measurements were performed using an Eclipse Ti-S inverted fluorescence microscope (Nikon Industries, New York, NY) equipped with a digital camera (Orca Flash 4.0, Hamamatsu Corp., Bridgewater, NJ). All images were processed using NIS-Elements 4.6 software (Nikon). Cell lysis videos were recorded at a frame rate of 15 fps. For enzymatic assay experiments, multichannel images using DIC, Texas Red, and green fluorescence filters were recorded at fixed exposure rates of 20 ms, 40 ms, and 40 ms respectively.

**Image processing.** During the voltage sweep for current-voltage measurements, the video was recorded at frame rates of

10-13 fps. The recorded file was converted into sequential images using an image software (ImageJ 1.52.a). EFs were calculated using MATLAB R2019b. For all the images, noise was removed by using the median filter function. The mask for each droplet was created from the initial image ($t$ = 0 min) captured using Texas Red filter that exhibited a uniform concentration distribution. Image opening and closing were applied for improved identification of the droplet interface. The resulting grey scale images were converted into binary images, which were then used for masking the corresponding images. The EFs were calculated by taking the ratio of the maximum intensity to the average initial intensity of the droplet and subtracting the background intensity (average intensity across an empty microchannel).

$$EF = \frac{[\max(I^t) - I_B]}{\left[\frac{\sum_N I_i^0}{A} - I_B\right]}$$

where $I^t$ and $I_B$ were the pixel intensity and background intensity, respectively for a timepoint $t$, and $A$ is the area of the droplet at $t$ = 0 min.

**Microplate reader assay for the optimization of substrate concentration.** Availability of excess substrate is a critical factor for evaluating β-galactosidase activity so that the rate of product formation is limited solely by the concentration of the enzyme. Therefore, the concentration of fluorescein conjugated beta-D-galactopyranoside (FDG), ranging from 0.5-2.0 mM was initially tested in enzymatic assays using microtiter plates. Subsequently, 1.0 mM FDG was identified as the optimal concentration for β-galactosidase assay at the nanoliter scale. The assay conditions were set to 37 ºC and the fluorescence response was monitored over a period of 45-60 min (Supporting Information, Figure S4).

## RESULTS AND DISCUSSION

**Device design and characterization.** The design and operation of the droplet microfluidic system are illustrated in Figure 1. Our device incorporates a main channel, with a droplet generation zone and a downstream electrokinetic zone, where the droplets are exposed to an applied voltage across cation exchange membranes (CEMs). These CEMs place the droplets in ionic communication with electrolyte-filled auxiliary channels, which flank the main channel. The voltage is applied between wire leads immersed in the inlet reservoirs of the auxiliary channels ("anode" and "cathode", Figure 1a) to establish a potential drop across the CEMs, with polarity as indicated in Figure 1d,e.

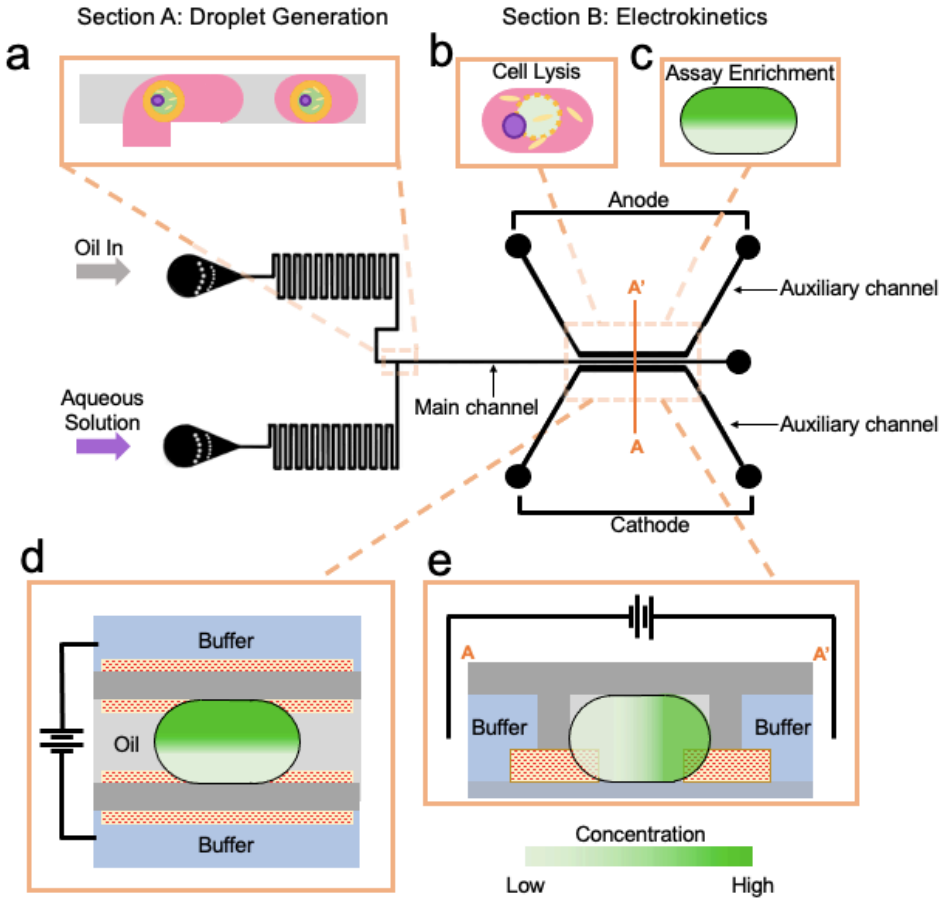


**Figure 1.** Schematic illustration of device design and operation. (**a**) Generation of droplets encapsulating cells, at a microfluidic T-junction. The droplets are flowed along the main channel and stationed between parallel cation exchange membranes that interconnect the droplets with electrolyte-filled auxiliary microchannels. Within the electrokinetic section of the device, ICP (**b**) drives cell lysis and (**c**) locally enriches assay products – here, a green fluorophore. (**d**) Top view and (**e**) cross-sectional view of a droplet undergoing ICP.

To characterize the in-droplet ICP-driven concentration enrichment, we evaluated the distribution of a model fluorophore (Texas Red-dye conjugated albumin) and measured the current across the electrokinetic zone. A detailed account of the experimental procedure and results are provided as Supporting Information, Note 2 and Figure S5). The distribution of the fluorophore with voltage ramping indicates the effect of voltage magnitude on the concentration enrichment (Supporting Information, Figure S6 and Movie S1).

**In-droplet electromechanical cell lysis.** ICP has been previously leveraged to facilitate the lysis of bacterial pathogens.[13] Kim and coworkers demonstrated ICP-driven recovery of lysate (including proteins and nucleic acids) from bacteria that were continuously flowed and lysed in a single (aqueous) phase within a microfluidic channel. Our current work accomplishes ICP-driven electromechanical cell lysis within nanoliter-scale water-in-oil droplets. To investigate this phenomenon, MDA-MB-231 breast cancer cells were suspended in a solution composed of 10.0 µM BSA-conjugated Texas Red anionic tracer (10% v/v), OptiPrep density modifier (17% v/v), and 1X DPBS buffer (73% v/v). The cells were pre-stained with Calcein AM, a green fluorescent dye that is activated by esterases present in the cell cytosol. Droplets encapsulating cells were generated at the T-junction and flowed to the electrokinetic zone of the device. The flow was stopped to station the droplets between the CEMs. The auxiliary channels were filled with a solution of 200.0 mM Tris·HCl buffer (pH 8.1, conductivity 9.8 mS/cm). A DC voltage of 50 V was applied between the two auxiliary channels (via their inlet reservoirs) and maintained for 10 s. This voltage application resulted in the dispersion of the calcein dye across the droplet, indicating rapid (~1-2 s) lysis of the encapsulated cells (Supporting Information, Movie S2). Cell lysis is attributed to ICP-driven electroconvection, which renders mechanical shear stress on cells, and elevated electric field strength, which causes electroporation. These effects were reported by Kim and coworkers for bacterial cells, but here, within confined volumes, cells are unable to escape these electromechanical effects.[13]

Figures 2a-c are composite images of overlaid green and red fluorescence micrographs taken before, during, and after ICP-driven cell lysis. The in-droplet ionic concentration distribution was monitored by using dye-linked BSA as the anionic tracer suspended in the droplet media. Figure 2a shows droplets encapsulating cells (bright circular spots) and having a uniform concentration distribution of ions in the absence of any electric field. Before lysis, the encapsulated cells are intact, exhibiting high green fluorescence intensities (due to encapsulated calcein dye) and having well-defined cell boundaries. With voltage application, the cells drift within the droplet, tending to move towards the cathodic end of the droplet under ICP-induced electroconvective force, and are eventually lysed. Concentration redistribution as indicated by the formation of IDZs and IEZs confirms the accomplishment of ICP within the droplets (Figure 2b). The droplets were imaged 30 s after switching off the voltage. Figure 2c shows release of cell contents (brightness and contrast were adjusted to view diffused green fluorescence from lysed cells) with an increase in the overall droplet intensities due to the dispersion of the calcein dye.

The cell lysis experiments were repeated in an isotonic lower conductivity buffer (~10-fold lower conductivity than 1X DPBS) at a lower voltage of 30 V (for 10 s) and similar results were obtained (Supporting Information, Movie S3). The buffer composition was changed to make it less electrically conductive to minimize any interference to ICP-driven enrichment caused by electrolyte ions. In our previous study, it was demonstrated that in-droplet ICP-driven enrichment negatively correlates with the electrolyte concentration.[12] Figure 3 shows fluorescence images obtained before (Figure 3a), during (Figure 3b), and after (Figure 3c) electromechanical lysis of three cells encapsulated within a single droplet. Figure 3b was obtained at $t = 27$ s after initiation of an applied voltage of 30 V and shows the development of IDZs as dark regions within the droplet. Figure 3c (right) shows the dispersion of the cell dye upon cell lysis. Additionally, increased cell diameters and turgidity post voltage application substantiate cell lysis. The in-droplet distribution of green fluorescence intensity from cells before and after voltage application, are plotted in Figure 3d,e. From these 3D colormaps, it is evident that the high fluorescence intensities associated with cells significantly diminish as the cells are lysed and the dye disperses.

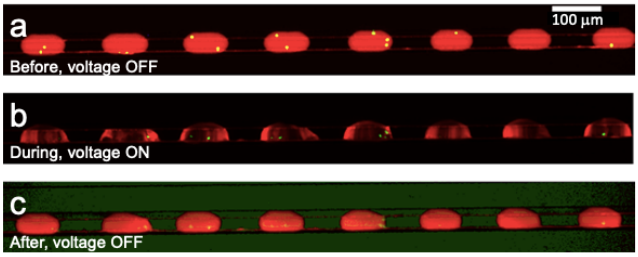


**Figure 2.** Composite red and green fluorescence micrographs (a) showing intact MDA-MB-231 cells (green spots) encapsulated in droplets containing Texas Red dye-linked BSA solution, in the absence of an externally applied electric field, (b) IDZ formation, electroconvective vortices, and cell lysis during the application of a voltage bias of 50 V, and (c) resulting cell lysis (debris and released green cytosolic dye) after switching off the voltage (the image brightness and contrast were adjusted to visualize green dye).

It was noted that the cells preferably lyse at the cathodic (lower) end of a droplet. Additionally, in the absence of fluidic recirculation (stationary droplets), the lysate debris was observed to adhere momentarily to the cathodic membrane. To characterize the cell lysis location quantitatively, fluorescence images captured during lysis were evaluated in terms of the $y$-distance of the cells from the cathodic membrane. Details of estimating the lysis location are provided in Supporting Information, Note 3 and Figure S7. It was found that most cells (25 out of 32) underwent lysis at a $y$-distance <25 µm, which was the width of the cathodic membrane overlapping with the droplet. This localized lysis is attributed to the development of IDZs, which establish hypotonic conditions, and fluidic vortices exerting shear stress at the cathodic end of the droplet. Additionally, the electric field strength is the highest at the cathodic membrane-droplet interface, which yields the highest transmembrane voltage across the cells. The relative importance of each of these factors to lysis is examined quantitatively by simulation in the next subsection. Furthermore, our investigation of the applied voltage (Supporting Information, Movies 4-7) shows that lower voltages (e.g., 4 V, 10 V) merely mobilize cells, while higher voltages (20 V, 30 V) lyse the cells at distinct lysis times. For example, a voltage bias of 20 V lysed a cell in 8 s, while 30 V lysed a cell at ~2 s. In addition to the applied voltage, we

hypothesize that the cell lysis time would also depend on factors such as a cell's location within the droplet, and the droplet shape or volume. For example, a cell drifting nearer to the cathodic CEM may tend to lyse more rapidly. Further, a cell encapsulated in a larger droplet may experience retarded electromechanical forces relative to that confined in a smaller (or geometrically compact) droplet, thereby increasing lysis time. Supporting Information, Figures S8 and S9 show the ICP response of distinct number of encapsulated cells. In the next subsection, we examine the spatial distribution of factors (electric field strength, ionic strength, shear stress) that contribute to cell lysis.

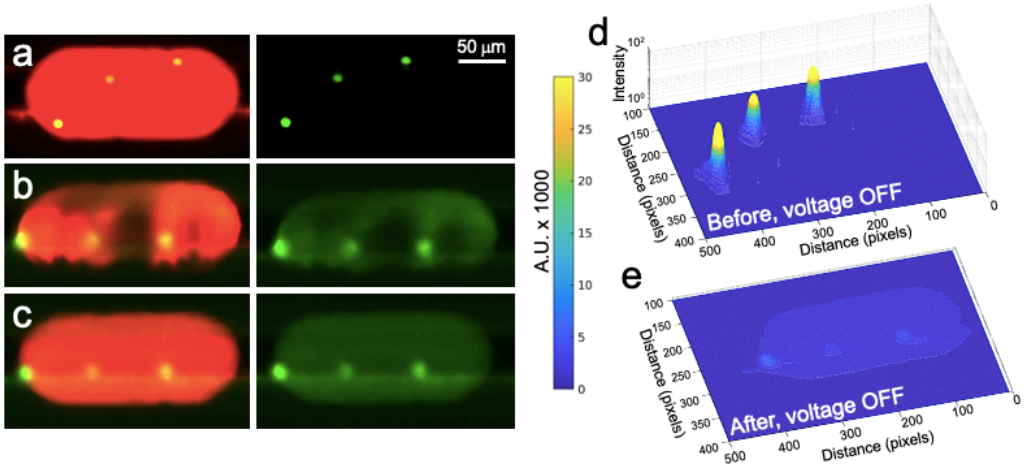


**Figure 3.** Electromechanical cell lysis in nanoliter-scale droplets. Overlaid green and red fluorescence micrographs (left), and corresponding green fluorescence micrographs (right) obtained (a) before, (b) during (at $t$ = 27 s), and (c) after cell lysis ($t$ = 60 s) for a droplet containing three cells. Voltage bias (50 V) applied at $t$ = 0 s. 3D contour plots showing the distribution of green fluorescence intensities (d) before and (e) after cell lysis.

**Simulation of in-droplet electrokinetic response.** We numerically studied droplet electrokinetics to understand electromechanical cell lysis and ICP-driven increases in sensitivity due to enrichment. The simulation was performed by solving the coupled Navier-Stokes and Poisson-Nernst-Planck equations (NS-PNP). The fluid momentum within the droplet can be expressed by the Navier-Stokes equation:

$$\rho\left(\frac{d\boldsymbol{u}}{dt}+\boldsymbol{u}\cdot\nabla\boldsymbol{u}\right)=-\nabla p+\eta\nabla^2\boldsymbol{u}-\rho_e\nabla\emptyset$$

where $\rho, \boldsymbol{u}, p, \eta, \rho_e$, and $\emptyset$ are density of fluid, velocity vector, pressure, viscosity, and charge density, and electric potential. The last term is responsible for the body force on the fluids from the electric field. In this study, we assume the fluid is divergence-free:

$$\nabla\cdot\boldsymbol{u}=0$$

The Nernst-Planck equation describes the mass transport of species $i$ under an applied electric field:

$$\frac{dc_i}{dt}+\boldsymbol{u}\cdot\nabla c_i=\nabla\cdot\left(D_i\nabla c_i+z_iD_i\frac{\mathrm{F}}{\mathrm{R}T}c_i\nabla\phi\right)$$

$c_i, D_i, z_i, \mathrm{F}, \mathrm{R}$, and $T$ are concentration, diffusivity, valence charge, Faraday constant, ideal gas constant, and temperature. Introducing the Poisson equation closes the problem:

$$-\varepsilon\nabla^2\phi=\rho_e$$

where $\varepsilon$ is the solution permittivity and $\rho_e$ is the charge density. The charge density can be expressed in terms of the local concentration of cations and anions for $N$ number of species,

$$\rho_e=\mathrm{F}\sum_{i=1}^{N}z_ic_i$$

The non-dimensional forms and numerical methods to solve the above governing equations were described in detail in our previous work.[14] In short, we use the finite element method to solve the coupled set of NS-PNP equations. At each time step, we perform block iteration between NS and PNP until convergence is achieved. That is, NS and PNP were solved separately, and the coupling terms updated after each block. We iterate until the solution (at that particular time-step) does not change with further block iteration. We use a second order time-stepper. A variational multiscale method (VMS) approach that ensures numerical stability is utilized. In addition, octree-based adaptive meshing ensures minimum computational costs while resolving the smallest length scale.

Our numerical study focuses on the behavior of the background electrolyte (phosphate buffer, 10.0 mM) in the droplet without cells or tracers. The fluid velocity at the oil-water interface was assumed to be zero, which is a good approximation for stationary droplets considering the viscosity jump at the interface. The non-dimensional cation concentration at the membrane was estimated to be 1, and no-mass flux across the membrane was assumed for the anion.

The simulation results for four distinct in-droplet parameters at an applied potential drop of 5.17 V are shown in Figure 4. This voltage is appropriate since only a fraction of the bias applied to the device is distributed across the droplet. The enrichment and depletion zones were confirmed from the distribution of the ionic strength, $I=\frac{1}{2}(c_+ + c_-)$ (Figure 4a, Supporting Information, Movie S8). In addition, the irregular interface of the depletion zone and complex flow streamline structures (Figure 4b, Supporting Information, Movie S9) indicate electrohydrodynamic instabilities in the droplet. Despite the low Reynolds number of the system under study, $Re \ll 1$, the instability is expected. Druzgalski et al. performed direct numerical simulations of the NS-PNP equations near a permselective membrane.[15] In their study, they showed that the high potential drop across an extended space charge layer (ESC) triggers instabilities even in a very small $Re$ regime. It is

noteworthy that the highest electric field strength and shear stress was found near the lower (cathodic) membrane (Figure 4c,d), which correlates with the cell lysis location discussed in the previous section. From the simulation, the estimated threshold value of shear stress at the bottom of the droplet (>50 Pa, Supporting Information, Movie S10) exceeds the reported value for lysing mammalian cells (>20 Pa).[16] Thus, shear stress plays a significant role in the lysis process. Note that at the droplet boundary, we assume a no slip condition despite the liquid-liquid interface there, which allows for slip. However, due to the high viscosity of the continuous (oil) phase, this simplifying assumption has a minimal impact on the accuracy of the simulation. Also, the electric field strength estimated for our system (~250 kV/m at the cathodic end, Supporting Information, Movie S11) is greater than the reported threshold for electrical cell lysis (~45 kV/m for a 20 $\mu$m-diameter cell).[17] While hypotonicity within the IDZ can induce lysis, the effect (swelling and bursting) is slower than either mechanical or electrical lysis. Therefore, it can be concluded from the simulation results that cell lysis in the droplet was mainly induced by the combined contributions from the high electric field and shear stress near the cathodic membrane.

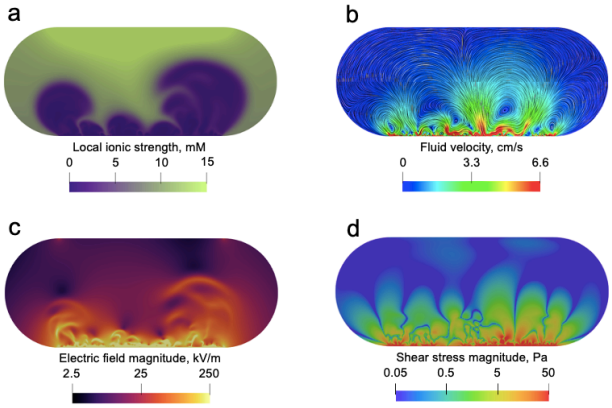


**Figure 4.** Simulation results for in-droplet (a) local ionic strength (mM), (b) fluid velocity (cm/s) (c) electric field strength (kV/m), and (d) fluid shear stress (Pa).

**Enhanced sensitivity and speed of a beta-galactosidase assay.** We next demonstrate the applicability of ICP-driven enrichment to enhance in-droplet beta-galactosidase enzymatic assay that follows cell lysis, in two different ways - by increasing the reaction rate and by amplifying the optical signal from the assay product. Therefore, ICP not only expedites assay detection (shortens processing time), but also improves the limit of detection (LOD). Beta-galactosidase is an intracellular enzyme commonly found within the lysosomal lumen and perinuclear region in mammalian cells. Lysosomal beta-galactosidase is a widely-used biomarker for cell senescence.[18] As a reporter enzyme, beta-galactosidase has been associated with the pathological assessment of various types of cancer.[19–22]

Droplets encapsulating MDA-MB-231 breast cancer cells in assay mixture containing fluorogenic FDG substrate (1.34% v/v, 1.0 mM), Mg++ buffer (1.34% v/v, containing 0.001 mM $MgCl_2.6H_2O$ and 0.067 M beta-mercaptoethanol), low conductivity buffer (70.4% v/v, see *Materials and Methods* for composition), OptiPrep (17% v/v), and Texas Red dye-linked BSA (10% v/v), were generated. ICP-driven cell lysis (30 V, 30 s) released beta-galactosidase into the encompassing droplet solution, triggering the hydrolysis of FDG substrate to fluorescein. Though cell lysis can be achieved by applying the voltage for a shorter time (1-2 s), a longer duration (30 s) of voltage application ensured complete lysis of drifting cells while providing time for image acquisition. At 1 min post the voltage being switched off, an image was captured. The microscope stage incubator was then switched on to externally start heating the chip to 37 °C. From 5-25 min, the chip was incubated at 37 °C in the absence of any electric field, and images were acquired over 5-min intervals.

To monitor the assay progress over time, the average intensity in the droplet (AID) was calculated.

$$AID = \frac{[(I_t - I_B^t) - (I_0 - I_B^0)]}{A_t}$$

where $I_t$ is the pixel intensity sum and $I_B^t$ is the average background intensity over the projected droplet area at $t = t$ min. $I_0$ and $I_B^0$ are the pixel intensity sum and average background intensity over the projected droplet area, respectively at $t$ = 0 min. $A_t$ is the projected droplet area at $t = t$ min. Therefore, AID is the spatial average of background subtracted intensity and is directly proportional to the amount of enzymatic reaction product (such that, change in AID over time indicates the reaction rate). In-droplet concentration enrichment is known to reach equilibrium in tens of seconds because enrichment of the product draws from a limited volume (i.e., the droplet).[12] Therefore, the collection and quantification of data has been performed by allowing sufficient time for the in-droplet enrichment to reach a steady state. Figure 5a shows the AID profile over time for a droplet initially containing four cells. At the start of this experiment ($t$ = 0 min), a voltage bias of 30 V was applied for 30 s, and the droplet was imaged during the resulting cell lysis (the data related to this step is depicted at $t$ = 0.5 min). Subsequently, the AID increased linearly indicating the gradual progression of the enzymatic reaction. At $t$ = 27 min, 30 V was applied for 30 s to locally concentrate the droplet contents. The green arrow in Figure 5a shows a discontinuity, corresponding to a sudden increase in AID during the voltage application at 27 min. This discontinuity implies an enhancement in reaction rate during voltage application and is attributed to concentration enrichment of the enzyme by ICP. From Figure 5a, this reaction rate, as depicted by the slope between $t$ = 25 min and $t$ = 29 min was estimated to be 5.22 A.U./min (3.8X the initial rate). This result demonstrates an increase in enzymatic reaction rate driven by concentration enrichment.

An increase in reaction rate after 27 min (slope = 2.67 A.U./min, Figure 5a, between $t$ = 29-37 min) compared to that before the readout (1.37 A.U./min, Figure 5a, between $t$ = 10-25 min) could potentially be attributed to ICP-induced pH and temperature changes. We have not yet developed a quantitative method to evaluate enzyme dynamics (e.g., turnover frequency) in the context of in-droplet ICP. This topic will be the focus of a future study from our laboratory. However, factors impacting enzyme dynamics such as, concentration enrichment (of the enzyme) and ICP-induced pH changes have been evaluated. We performed a control experiment to evaluate droplet pH (Supporting Information, Note 4 and Figure S10). Droplets containing 10.0 mM phosphate buffer and universal pH indicator were subjected to ICP (30 V applied voltage) for 1 min. With ICP and exposure of a droplet to the CEM, which is acidic, the droplet pH is expected to decrease. However, ICP-

induced pH changes were not visually detectable. The droplets containing phosphate buffer still appeared green after ICP, while the Nafion membranes appear red (acidic) throughout the experiment. Therefore, we concluded that the buffering capacity is sufficient to prevent extensive acidification of the droplets. Further, to evaluate the effect of pH on the enzymatic assay response, the assay was carried out in 1X DPBS solutions having distinct pH using a microplate reader. A greater increase in fluorescence intensity was obtained at pH 6.2 and 7.4 compared to pH 7.8 and 8.2 (Supporting Information, Note 5 and Figure S11). We further tested assay response in distinct buffers and found out that Tris buffer extensively suppressed beta-gal activity (Supporting Information, Note 6 and Figure S12). These results underscore the importance of maintaining consistent droplet pH and selecting an appropriate buffer. We next evaluated the enhancement in sensitivity afforded by ICP-based enrichment of the assay product at readout. Figure 5b is a plot of the maximum intensity in droplet, MID, which was evaluated from the same data as Figure 5a. The MID was calculated by averaging the background subtracted intensity of the brightest region of interest (2 pixels x 2 pixels) in the intermembrane region. From $t$ = 0-25 min, MID increased gradually, however, the signal was increased 19-fold by ICP at readout (27 min). The fold enrichment was calculated by dividing the MID value at readout (27 min) by the AID just before the readout (25 min). The AID and MID for three droplets that encapsulate a variable number of cells is provided in Supporting Information, Figure S13. In all cases, irrespective of the number of encapsulated cells, an increased sensitivity at readout was observed. However, the intensity values did not correspond proportionally to the number of cells. For example, the product fluorescence from 2 cells was expected to be lower than that from 3 cells, but it was not the case. This distribution in intensities may stem from cell heterogeneity or non-uniform localized concentration distribution between droplets. For quantifying the contribution of cell heterogeneity in intensity distribution, a uniform electrokinetic response across all the droplets is necessary. Device designs enabling such a response will be the focus of future studies. For example, less variability in enrichment is expected in devices that generate droplets with more consistent volumes and that have more uniform CEM thickness.

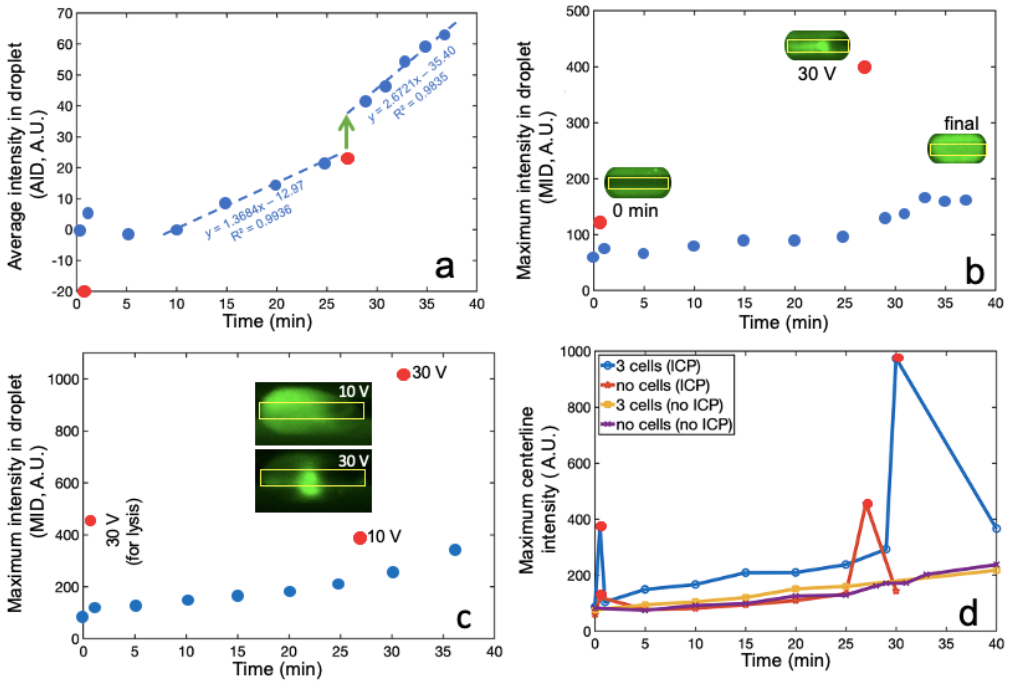


**Figure 5.** (a) Distribution of average intensity in a droplet (AID, A.U.) that initially contained four cells, over the experiment duration. A voltage bias of 30 V was applied at $t$ = 0.5 min to lyse the cells and then applied again at $t$ = 27 min (readout). Red circles indicate datapoints obtained during voltage application. The blue dashed lines show the rate of increase in intensity, which is proportional to reaction rate, prior to and post readout. (b) Distribution of maximum intensities (MID, A.U.) over time for the same droplet. Insets show green fluorescence micrographs of the droplet at the stated time points with the inter-membrane region considered for MID estimation. (c) Plot showing the MID distribution over time for a droplet that initially contained three cells. A voltage bias of 30 V was applied at $t$ = 0.5 min for cell lysis, 10 V was applied at 27 min, and 30 V was applied again for readout at 31 min. The droplet is half as enriched at 10 V (4.7-fold) compared to at 30 V (9.7-fold). Insets are fluorescence micrographs of the droplet at each of the two readout voltages (10 V and 30 V). (d) Background-subtracted maximum intensities taken across the droplet centerline for droplets with distinct conditions of cell encapsulation and electrokinetics (ICP). The data points highlighted with red circles indicate voltage application of 30 V. It can be noted that the intensity values as well as intensity increase over time with ICP (blue trace) was much higher compared to the controls without ICP (purple and yellow traces) or without cell encapsulation (purple and red traces).

To investigate the effect of the magnitude of applied voltage on the signal enhancement at readout, we evaluated concentration enrichment at two voltage conditions -10 V and 30 V. Figure 5c is a plot of the maximum intensity profile over the duration of an enzymatic assay carried out in a droplet containing three cells. At $t$ = 0 s, a voltage bias of 30 V was applied for 30 s to

lyse the cells. Thereafter, the device was incubated at 37 °C before applying a voltage of 10 V at $t$ = 27 min. The voltage application was then stopped before applying 30 V for a second readout at $t$ = 31 min. It was found that the signal enhancement was ~9.7-fold higher at 30 V compared to 4.7-fold at 10 V. Therefore, the fold-enrichment was twice with an applied voltage of 30 V compared to 10 V. The AID and MID for two droplets (within the same device) that encapsulate a variable number of cells is shown in Supporting Information, Figure S14. It was observed that the signal enhancement obtained at 10 V was 1.6-2X lower compared to that at 30 V in all the cases. These results are in agreement with the conclusion that concentration enrichment increases with the magnitude of the applied voltage.[12] For a given channel geometry and droplet volume and composition, the applied voltage at readout must be optimized to enable maximum sensitivity with ICP. A very low voltage bias can lead to inefficient enrichment (or take a longer duration to accomplish ICP) whereas very high voltages can disperse the enriched analyte due to fluidic instabilities and vortices.

A series of control experiments were performed to evaluate for false positive contributions to signal intensity arising from non-specific substrate hydrolysis (non-enzymatic). For all the control experiments, the background-subtracted green fluorescence intensities across the horizontal midline of a droplet were profiled. These centerline intensities exclude the superfluous intensity from the overlap of a droplet with the CEMs that exhibit some inherent fluorescence. Figure 5d compares the maximum pixel intensities along this centerline for four droplets without and with ICP both in the absence and presence of cells. With no cells encapsulated, and without ICP, a negligible increase in the intensity was observed (purple trace). This result is expected for this negative control. In the absence of ICP, a droplet encapsulating cells showed a similar gradual increase in intensity over the experiment duration (yellow trace). This result is similar to that of the negative control owing to the absence of cell lysis and the consequent restricted access of the enzyme to the substrate. With ICP and in the absence of cells (red trace), the trace overlies the negative controls except under voltage application (indicated by red circles). Based on this result, we conclude that some non-specific hydrolysis of the FDG substrate occurred as evidenced by the higher peak in intensity at the second voltage application ($t$ = 27 min) than the first (applied at $t$ = 0.5 min for 30 s). Finally, with ICP, droplets encapsulating cells exhibit higher intensity values throughout the experiment and especially at readout due to the local enrichment of the formed assay product (blue trace). It should be noted that the signal intensities for the controls not employing ICP (purple and yellow) are insignificant compared to that observed with ICP (blue), especially at the readout. Therefore, ICP drives the local enrichment of the analyte and enhances the sensitivity multifold. The intensity values associated with non-specific hydrolysis (red trace, Figure 5d) were found to be lower than enzyme-driven hydrolysis. Typically, in the absence of external chip heating, the overall intensity values were found to be lower for distinct conditions of ICP and cell encapsulation (Supporting Information, Figure S15–S17). For example, under the conditions of ICP, no cells, but in the absence of externally applied heat, lower peak (130 vs. 457 A.U.) and final (94 vs. 144 A.U.) intensities were observed (Supporting Information, Figure S16a) compared to when external heat was applied to the chip (red trace, Figure 5d). This result indicates that temperature-driven FDG decomposition via external heating contributes significantly to non-specific hydrolysis.

To further quantify enzyme concentration, a calibration curve was obtained both with and without electrokinetic enrichment using known quantities of purified beta-gal under conditions matched to those employed for cell analysis. The experimental details are included in the Supporting Information, Note 7 and Figure S18. These results can be utilized to estimate the enzyme activity in analyzed cells, and they illustrate both the sensitivity gained by ICP and the magnitude of droplet-to-droplet variation.

We further investigated the ICP-driven enhancement of assay sensitivity with intermittent voltage application. The detailed procedure and results are included in Supporting Information, Note 8 and Figure S19. With intermittent voltage application, the AID and MID for empty droplets (blank) as well as those encapsulating cells were evaluated. The results indicate that signal responses (in the presence of cells) obtained with ICP were well-distinguished from the corresponding LOD (with ICP) beyond a threshold time of $t$ = 23 min. Therefore, intermittent ICP can be used to sensitively determine signal responses from enzymatic assays.

## CONCLUSION

In this paper, ICP was characterized in nanoliter-scale water-in-oil droplets with compositions relevant to cell analysis. Three key applications that leverage this in-droplet ICP were demonstrated. First, we described ICP-driven rapid (in seconds) electromechanical lysis of MDA-MB-231 breast cancer cells encapsulated in droplets. Lysis was confirmed by the dispersion of a cytosolic fluorescent dye and was identified to invariably occur over the cathodic membrane, where the electric field strength and shear force were highest. Results from simulating the ionic strength, electric field distribution, and fluid dynamics within a droplet revealed that the electric field and shear stress at the cathodic membrane far exceeded that required for electromechanical lysis, thereby identifying them as the driving forces for lysis in our system. These results are important because ICP-based lysis on demand provides spatiotemporal control over lysis. Our method provides scope for high-throughput in-droplet lysis, lysis in moving droplets, and lysis of other cell types by optimizing the voltage and ICP-induced electromechanical effects.

Second, we demonstrated up to 19-fold amplification of the signal obtained during readout of an enzymatic assay by ICP-driven local concentration enrichment of the fluorescent product of the assay. We further quantified the degree of enhancement in sensitivity with intermittent ICP. With ICP, the signals beyond a threshold of 23 min were well-separated from the LOD, while in the absence of ICP, the signal remained below the LOD throughout the experiment (>40 min). This advancement is significant because this improvement in sensitivity will allow for the product to be detected either sooner or at a lower concentration. Given that an enzymatic reaction accumulates product linearly over time, and assuming that enrichment factor is independent of average concentration of the product, we estimate that the enzyme can be detected at an order of magnitude lower concentration than that without ICP. Finally, our results indicate that ICP-driven enrichment of in-droplet assay contents increases the enzymatic reaction rate by 3.8-fold.

Our method utilizes ICP to improve sensitivities and enable early detection of bioanalytes within nanoliter-scale droplets without any additional sample preparation steps. Further optimization of the design and current densities would yield more quantitative and reproducible results by accomplishing more uniform local concentration distribution across droplets.

## ASSOCIATED CONTENT

Supporting Information

The Supporting Information is available free of charge on the ACS Publications website.

Additional details on device dimensions (Note 1) and fabrication protocol including a scheme (Figure S1) and SEM images of membranes (Figure S2). Poisson distribution for cell encapsulation in a 1 nL droplet (Figure S3), plot showing fluorescence increase per minute for distinct substrate concentration for assay (Figure S4). Additional experimental details on characterization of in-droplet ICP-driven concentration enrichment (Note 2, Figure S5), ICP-based concentration distribution of Texas red-BSA at distinct voltages (Figure S6), cell lysis location including micrographs and plot (Note 3 and Figure S7), ICP response of multiple encapsulated cells (Figure S8 and S9). Model pH studies (Note 4 and Figure S10), effect of pH on enzymatic assay (Note 5 and Figure S11) effect of buffer composition on assay (Note 6 and Figure S12), MID and AID for droplets containing variable number of cells (Figure S13 (30 V), S14 (10 V and 30 V) with external chip heating. MID and AID for droplets without external chip heating – for droplets encapsulating variable number of cells with a voltage applied for cell lysis and at readout (S15), - in the absence of cells (S16, negative control), and in the absence of voltage application (S17). Calibration plot for quantitation of enzyme concentration (Note 7 and Figure S18), experimental details on enhancement in assay with intermittent voltage application (Note 8 and Figure S19). Movie files showing concentration distribution of anionic tracer (Movie S1), cell lysis at voltages 50 V (Movie S2), 30 V (Movie S3, S7), 4 V (Movie S4), 10 V (Movie S5), 20 V (Movie S6). Simulation videos of in-droplet ionic strength (Movie S8), flow velocity (Movie S9), shear stress (Movie S10), and electric field strength (Movie S11) at 5.17 V.

## ACKNOWLEDGMENT

Financial support through NSF CAREER grant awarded by the Chemistry Directorate Chemical Measurement and Imaging Program under award number 1849109 is gratefully acknowledged. We acknowledge partial support from NSF 2053760, and ONR N00014-19-1-2453 for developing the simulation framework, and NSF 2018594 and XSEDE/ACCESS for computing resources. Authors thank Anand group member Han Chen for SEM imaging. Authors thank the W. M. Keck Metabolomics Research Laboratory at Iowa State University for the microplate reader instrumentation.

## AUTHOR INFORMATION

**Corresponding Author**

*Robbyn K. Anand − *Department of Chemistry, Iowa State University, Ames, Iowa 50011-1021, United States;* orcid.org/0000-0003-2801-8280; Email: rkanand@ iastate.edu

**Authors**

Baskar Ganapathysubramanian − *Department of Mechanical Engineering, Iowa State University, Ames, Iowa 50011-1021, United States;* orcid.org/0000-0002-8931-4852

‡†Sungu Kim − *Department of Mechanical Engineering, Iowa State University, Ames, Iowa 50011-1021, United States;* orcid.org/0000-0001-7446-1123

‡Aparna Krishnamurthy − *Department of Chemistry, Iowa State University, Ames, Iowa 50011-1021, United States;* orcid.org/0000-0003-1123-1026

Pooja Kasiviswanathan − *Microbiology Undergraduate Program, Iowa State University, Ames, Iowa 50011-1021, United States;* orcid.org/*0000-0002-9668-7737*

*‡These authors contributed equally.*

**Present Address**

†Department of Mechanical Engineering, Stanford University, Stanford, California 94305, United States.

**Author Contributions**

R.K.A., S.K. and A.K. designed research; S.K. and A.K. performed research; S.K. and B.G. designed and performed computations; S.K. and A.K. curated and analyzed data; P.K. prepared microtiter plates and analyzed data for the optimization of substrate concentration for the enzymatic assay; S.K. and A.K. wrote the paper; B.G. and R.K.A. supervised research.

## REFERENCES

(1) Mashaghi, S.; Abbaspourrad, A.; Weitz, D. A.; van Oijen, A. M. Droplet Microfluidics: A Tool for Biology, Chemistry and Nanotechnology. *TrAC Trends Anal. Chem.* **2016**, *82* (September), 118–125. https://doi.org/10.1016/j.trac.2016.05.019.

(2) Suea-Ngam, A.; Howes, P. D.; Srisa-Art, M.; DeMello, A. J. Droplet Microfluidics: From Proof-of-Concept to Real-World Utility? *Chem. Commun.* **2019**, *55* (67), 9895–9903. https://doi.org/10.1039/C9CC04750F.

(3) Sohrabi, S.; Kassir, N.; Keshavarz Moraveji, M. Droplet Microfluidics: Fundamentals and Its Advanced Applications. *RSC Adv.* **2020**, *10* (46), 27560–27574. https://doi.org/10.1039/D0RA04566G.

(4) Janiszewska, M. The Microcosmos of Intratumor Heterogeneity: The Space-Time of Cancer Evolution. *Oncogene* **2020**, *39* (10), 2031–2039. https://doi.org/10.1038/s41388-019-1127-5.

(5) Xiao, Z.; Dai, Z.; Locasale, J. W. Metabolic Landscape of the Tumor Microenvironment at Single Cell Resolution. *Nat. Commun.* **2019**, *10* (1), 1–12. https://doi.org/10.1038/s41467-019-11738-0.

(6) Loponte, S.; Lovisa, S.; Deem, A. K.; Carugo, A.; Viale, A. The Many Facets of Tumor Heterogeneity: Is Metabolism Lagging Behind? *Cancers (Basel).* **2019**, *11* (10), 1574. https://doi.org/10.3390/cancers11101574.

(7) Yu, Z.; Zhou, L.; Zhang, T.; Shen, R.; Li, C.; Fang, X.; Griffiths, G.; Liu, J. Sensitive Detection of MMP9 Enzymatic Activities in Single Cell-Encapsulated Microdroplets as an Assay of Cancer Cell Invasiveness. *ACS Sensors* **2017**, *2* (5), 626–634. https://doi.org/10.1021/acssensors.6b00731.

(8) Dhar, M.; Lam, J. N.; Walser, T.; Dubinett, S. M.; Rettig, M. B.; Di Carlo, D. Functional Profiling of Circulating Tumor Cells with an Integrated Vortex Capture and Single-Cell Protease Activity Assay. *Proc. Natl. Acad. Sci.* **2018**, *115* (40), 9986–9991. https://doi.org/10.1073/pnas.1803884115.

(9) Ouyang, W.; Han, J. Universal Amplification-Free Molecular Diagnostics by Billion-Fold Hierarchical Nanofluidic Concentration. *Proc. Natl. Acad. Sci. U. S. A.* **2019**, *116* (33), 16240–16249. https://doi.org/10.1073/pnas.1904513116.

(10) Chen, C. H.; Sarkar, A.; Song, Y. A.; Miller, M. A.; Kim, S. J.; Griffith, L. G.; Lauffenburger, D. A.; Han, J. Enhancing Protease Activity Assay in Droplet-Based Microfluidics Using a Biomolecule Concentrator. *J. Am. Chem. Soc.* **2011**, *133* (27), 10368–10371. https://doi.org/10.1021/ja2036628.

(11) Saucedo-Espinosa, M. A.; Dittrich, P. S. In-Droplet Electrophoretic Separation and Enrichment of Biomolecules. *Anal. Chem.* **2020**, *92* (12), 8414–8421. https://doi.org/10.1021/acs.analchem.0c01044.

(12) Kim, S.; Ganapathysubramanian, B.; Anand, R. K. Concentration

Enrichment, Separation, and Cation Exchange in Nanoliter-Scale Water-in-Oil Droplets. *J. Am. Chem. Soc.* **2020**, *142* (6), 3196–3204. https://doi.org/10.1021/jacs.9b13268.

(13) Kim, M.; Wu, L.; Kim, B.; Hung, D. T.; Han, J. Continuous and High-Throughput Electromechanical Lysis of Bacterial Pathogens Using Ion Concentration Polarization. *Anal. Chem.* **2018**, *90* (1), 872–880. https://doi.org/10.1021/acs.analchem.7b03746.

(14) Kim, S.; Khanwale, M. A.; Anand, R. K.; Ganapathysubramanian, B. Computational Framework for Resolving Boundary Layers in Electrochemical Systems Using Weak Imposition of Dirichlet Boundary Conditions. *Finite Elem. Anal. Des.* **2022**, *205* (September 2021), 103749. https://doi.org/10.1016/j.finel.2022.103749.

(15) Druzgalski, C. L.; Andersen, M. B.; Mani, A. Direct Numerical Simulation of Electroconvective Instability and Hydrodynamic Chaos near an Ion-Selective Surface. *Phys. Fluids* **2013**, *25* (11), 110804. https://doi.org/10.1063/1.4818995.

(16) Ludwig, A.; Kretzmer, G.; Schügerl, K. Determination of a "Critical Shear Stress Level" Applied to Adherent Mammalian Cells. *Enzyme Microb. Technol.* **1992**, *14* (3), 209–213. https://doi.org/10.1016/0141-0229(92)90068-Y.

(17) Brown, R. B.; Audet, J. Current Techniques for Single-Cell Lysis. *J. R. Soc. Interface* **2008**, *5* (suppl_2). https://doi.org/10.1098/rsif.2008.0009.focus.

(18) Lee, B. Y.; Han, J. A.; Im, J. S.; Morrone, A.; Johung, K.; Goodwin, E. C.; Kleijer, W. J.; DiMaio, D.; Hwang, E. S. Senescence-Associated β-Galactosidase Is Lysosomal β-Galactosidase. *Aging Cell* **2006**, *5* (2), 187–195. https://doi.org/10.1111/j.1474-9726.2006.00199.x.

(19) Li, Z.; Ren, M.; Wang, L.; Dai, L.; Lin, W. Development of a Red-Emissive Two-Photon Fluorescent Probe for Sensitive Detection of Beta-Galactosidase in Vitro and in Vivo. *Sensors Actuators B Chem.* **2020**, *307* (December 2019), 127643. https://doi.org/10.1016/j.snb.2019.127643.

(20) Gu, K.; Qiu, W.; Guo, Z.; Yan, C.; Zhu, S.; Yao, D.; Shi, P.; Tian, H.; Zhu, W.-H. An Enzyme-Activatable Probe Liberating AIEgens: On-Site Sensing and Long-Term Tracking of β-Galactosidase in Ovarian Cancer Cells. *Chem. Sci.* **2019**, *10* (2), 398–405. https://doi.org/10.1039/C8SC04266G.

(21) Li, X.; Pan, Y.; Chen, H.; Duan, Y.; Zhou, S.; Wu, W.; Wang, S.; Liu, B. Specific Near-Infrared Probe for Ultrafast Imaging of Lysosomal β-Galactosidase in Ovarian Cancer Cells. *Anal. Chem.* **2020**, *92* (8), 5772–5779. https://doi.org/10.1021/acs.analchem.9b05121.

(22) Kubo, H.; Murayama, Y.; Ogawa, S.; Matsumoto, T.; Yubakami, M.; Ohashi, T.; Kubota, T.; Okamoto, K.; Kamiya, M.; Urano, Y.; Otsuji, E. β-Galactosidase Is a Target Enzyme for Detecting Peritoneal Metastasis of Gastric Cancer. *Sci. Rep.* **2021**, *11* (1), 10664. https://doi.org/10.1038/s41598-021-88982-2.

**For Table of Contents Only**